Annals of Biomedical Engineering (2023) 51:2258–2266
https://doi.org/10.1007/s10439-023-03265-3

BMES BIOMEDICAL ENGINEERING SOCIETY

ORIGINAL ARTICLE

The Use of Optical Tracking to Characterize Fracture Gap Motions and Estimate Healing Potential in Comminuted Biomechanical Models of Surgical Repair

A. Ammar[1] · A. Koshyk[2] · M. Kohut[1] · B. Alolabi[3] · C. E. Quenneville[1,2]

Received: 10 August 2022 / Accepted: 31 May 2023 / Published online: 9 June 2023

Abstract

Fracture healing is stimulated by micromotion at the fracture site, whereby there exists an optimal amount of strain to promote secondary bone formation. Surgical plates used for fracture fixation are often evaluated for their biomechanical performance using benchtop studies, where success is based on overall construct stiffness and strength measures. Integration of fracture gap tracking to this assessment would provide crucial information about how plates support the various fragments present in comminuted fractures, to ensure there are appropriate levels of micromotion during early healing. The goal of this study was to configure an optical tracking system to quantify 3D interfragmentary motion to assess the stability (and corresponding healing potential) of comminuted fractures. An optical tracking system (OptiTrack, Natural Point Inc, Corvallis, OR) was mounted to a material testing machine (Instron 1567, Norwood, MA, USA), with an overall marker tracking accuracy of 0.05 mm. Marker clusters were constructed that could be affixed to individual bone fragments, and segment-fixed coordinate systems were developed. The interfragmentary motion was calculated by tracking the segments while under load and was resolved into compression–extraction and shear components. This technique was evaluated using two cadaveric distal tibia–fibula complexes with simulated intra-articular pilon fractures. Normal and shear strains were tracked during cyclic loading (for stiffness tests), and a wedge gap was also tracked to assess failure in an alternate clinically relevant mode. This technique will augment the utility of benchtop fracture studies by moving beyond total construct response and providing anatomically relevant data on interfragmentary motion, a valuable proxy for healing potential.

Keywords Motion capture · Fracture plates · Fracture healing · Coordinate system

Introduction

After a bone is fractured, the healing process is influenced by both the biological and mechanical environments [12, 27]. The biological environment includes the condition of the host tissue and the blood supply to the fracture site, while the mechanical environment involves the applied forces and interfragmentary motion [12]. Although several factors, including the size of the fracture gap [3, 7, 18] and the frequency of the applied loads [11, 26], are known to influence healing, the mechanical stability and interfragmentary motion play a crucial role in determining the type of bone healing that will take place [7]. Primary bone healing will occur when there is minimal interfragmentary motion and a negligible gap size in between the fragments [3], whereas secondary bone healing occurs when the fracture gap is a moderate size and there is relatively less stability at the fracture site [3, 27]. Not only does secondary bone healing not require a rigidly stable fixation, but small amounts of micromotion can enhance the healing process [18]. Most fractures heal by secondary healing, which does a more thorough job of replacing old and damaged bone [3].

Many studies have developed relationships between the amount of motion at the fracture site and the resulting

Associate Editor Michael R. Torry oversaw the review of this article.

✉ C. E. Quenneville
quennev@mcmaster.ca

[1] School of Biomedical Engineering, McMaster University, Hamilton, ON, Canada

[2] Department of Mechanical Engineering, McMaster University, Hamilton, ON, Canada

[3] Division of Orthopaedic Surgery, Department of Surgery, McMaster University, Hamilton, ON, Canada

healing. This motion can be represented by the strain at the fracture site, which is defined as the relative change in the size of the fracture gap divided by the initial size of the fracture gap [7]. To achieve the necessary stability and promote healing, surgical plates used for fracture fixation are often used to provide either absolute or relative stability [9]. Absolute stability leads to virtually no relative motion between the bone fragments, with strains below 2%, and promotes primary bone healing [9]. Relative stability allows small amounts of motion at the fracture site and leads to higher levels of strain, typically between 2 and 10%, and promotes secondary bone healing [7, 9]. However, if there is too much instability at the fracture site leading to excessive strains, the fracture will not be able to heal [12, 14, 22]. Other work has shown that axial interfragmentary movements as small as 0.2 mm are sufficient to stimulate callus formation, while larger movements of up to 1 mm can also be tolerated [2]. Additionally, in the presence of small axial movements of approximately 0.5 mm, shear interfragmentary movements below 0.8 mm have been reported to facilitate optimal healing [23].

This idea that three-dimensional interfragmentary motion plays an important role in bone healing has long been accepted [8]. Existing work involving benchtop biomechanical models to assess immediate post-surgical stability has relied upon axial and torsional stiffness measurements as an alternative to fracture site motion [21, 28], even though its relation to interfragmentary motion and bone healing is unclear [8]. Although some work has found stiffness measurements to agree with the amount of displacement at the fracture site [21], other work found construct stiffness to be a poor substitute for fracture site motion and concluded that three-dimensional interfragmentary motion should instead be used in governing implant design and operative fixation strategies [8]. Other studies have quantified the gaps of the fracture and monitored interfragmentary movements using optical tracking during the early healing stage [6]. However, this technique is more invasive which requires surgically attaching markers to participants using Schanz screws and Ilizarov ring [6]. Although several studies have attempted to apply optical systems to this problem [4, 10, 17, 20], determining the optimal mechanical environment for secondary fracture healing is still largely limited by an inability to measure fracture site motion for different types of fractures, including line and wedge fractures, that involve compressive, shear, and angular interfragmentary movements [8]. Therefore, the purpose of this study was to develop a technique to track three-dimensional interfragmentary motions at a fracture site and resolve them into normal, shear, and angular components for anatomically relevant outcomes while a repaired bone construct was loaded to simulate the immediate post-repair condition for healing.

Methods

Interfragmentary Motion Capture System

This technique integrated a three-dimensional optical tracking system (to characterize interfragmentary motion) with a material testing machine (to conduct benchtop loading of *ex vivo* repaired specimens) and will be described throughout this paper in terms of how it was implemented on two comminuted fractured and repaired distal tibia and fibula complexes, although it could be applied to any fractured specimen. The work described was approved and conducted in accordance with the Hamilton Integrated Research Ethics Board (HiREB 1946).

Four cameras (Flex 13, OptiTrack, Natural Point Inc., Corvallis, OR) were used to provide 360° tracking around a specimen and were supported using a welded steel tube frame. The frame was secured to a material testing machine (Instron 5967, Norwood, MA, USA) with the goals of minimizing vibrations and optimizing the capture volume (45 cm × 35 cm × 45 cm) for a repaired specimen (Fig. 1). All reflective surfaces present within the capture volume, including the fracture plates, screws, and the frame of the materials testing machine were covered in matte black paint or black fabric to prevent them from interfering with the tracking of the markers.

The optical tracking system was calibrated using a calibration wand (CWM-125 Calibration Wand, OptiTrack, Natural Point Inc, Corvallis, OR), and the origin was defined at the edge of the material testing machine base (with *X*-axis to the back, *Y*-axis vertical, and *Z*-axis to the right). The total estimated error for the system was calculated by the software (Motive, OptiTrack, Natural Point Inc., Corvallis, OR). Finally, a digitizing probe (MSP0001, OptiTrack, Natural

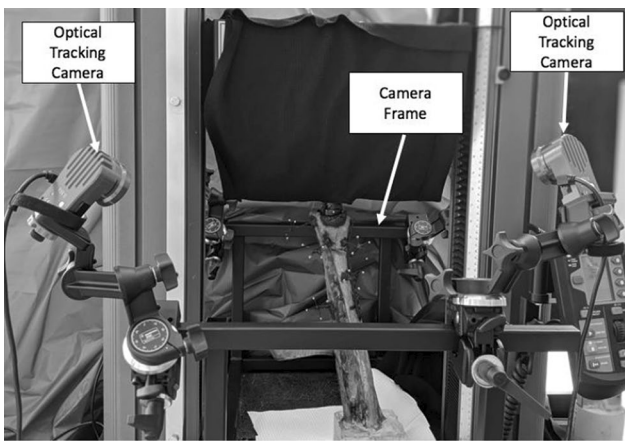

Fig. 1 Test setup with four cameras supported by a welded frame and positioned around the working area of a materials testing machine

Point Inc., Corvallis, OR) was registered to the setup using a calibration bar (CB-300 Calibration Bar, OptiTrack, Natural Point Inc., Corvallis, OR).

Reflective, spherical markers (6.4 mm in diameter) were used to track the motion of each bone fragment (assumed as rigid bodies). As such, clusters were developed to establish a local coordinate system for each fragment (Fig. 2). This extended the markers off the surface of the bone to ensure unobstructed tracking and was custom made using toothpicks, cotter pins, and hot glue to minimize the weight (approximately 1.2 g). Four markers were used in each cluster to mitigate the impact of potential obstructions. Small holes were drilled (3/32" diameter) into each bone fragment to allow for the clusters to be inserted and glued in place. Virtual points were then digitized relative to each cluster using the digitizing probe, which was done at both ends of the fracture, on both sides of the gap (Fig. 2) to facilitate tracking the fracture gap motions in 3D, which could then be translated into compression, shear, and angulation components.

Error Analysis

The accuracy of the optical tracking system was directly compared to a micrometer. A toothpick was taped to each side of the micrometer and a reflective marker was glued to the end of each toothpick. Measurements were taken in both the horizontal and vertical directions at nine locations in the transverse plane and three different heights to characterize the entire capture volume area of interest (Fig. 3). The micrometer was adjusted a fixed amount, ranging from

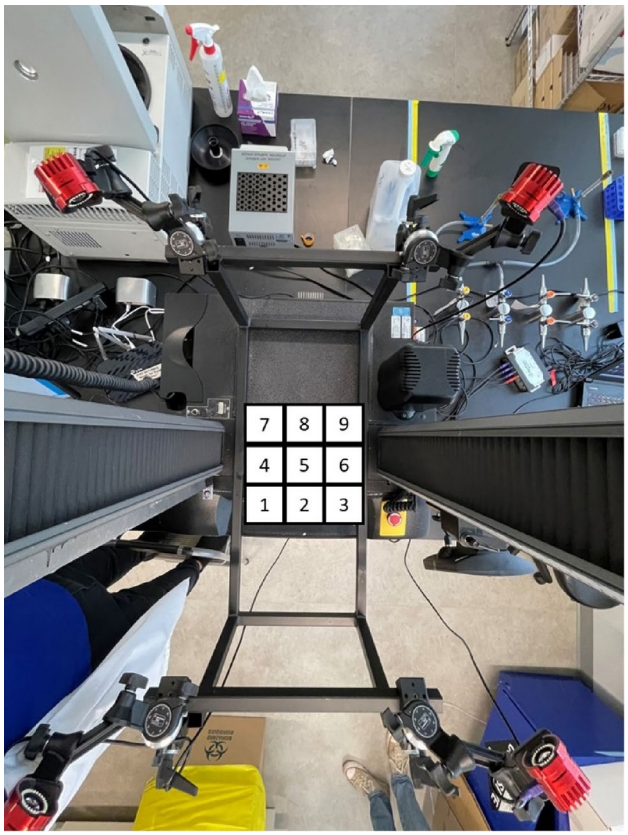

Fig. 3 Overhead view of the locations where the error analysis was conducted (looking down). The error at each of these nine locations was measured at three different heights

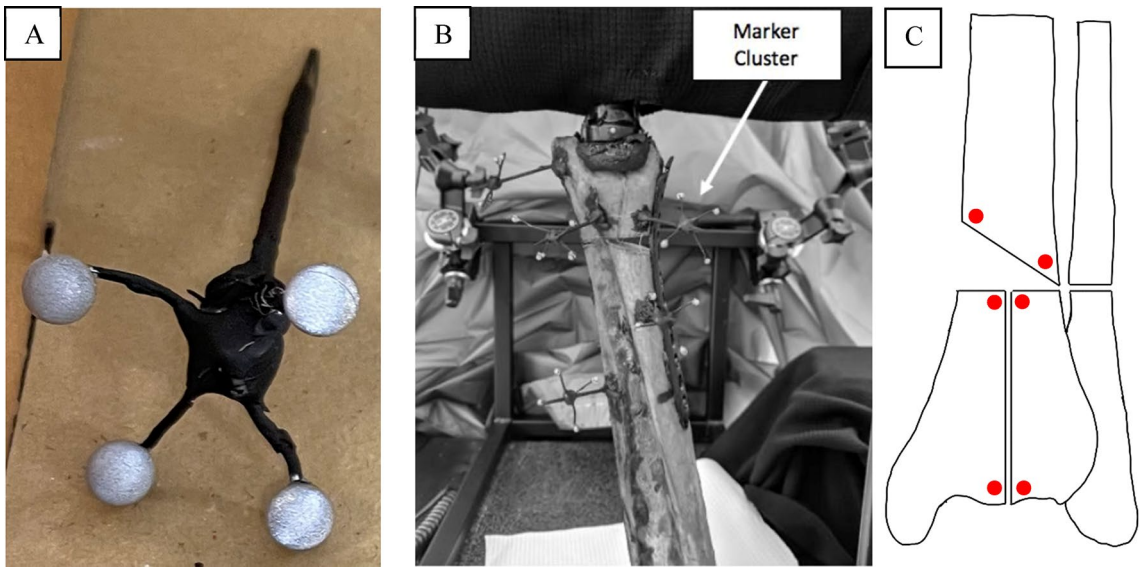

Fig. 2 **a** Marker cluster set created using four reflective markers (of 6.4 mm diameter) and **b** one cluster was secured to each bone fragment in the complex. **c** Virtual points, shown in red, were placed at both ends and on either side of the fracture gaps

0.5 to 3 mm, and the displacement from the micrometer was compared to the displacement reported from the optical tracking system.

To assess the level of noise induced by the vibrations from the material testing machine, two markers were secured within the center of the capture volume and a ten-second static test was conducted. This was followed by a 10-second dynamic test where the Instron head was operating at a rate of 0.1 mm/s. As there was no contact between the marker clusters and the Instron head during either the static or dynamic test, the markers remained stationary, and the amount of noise induced by the material testing machine during operation was defined as the maximum displacement of the markers throughout each test.

To evaluate the internal stability of the custom-made marker clusters, the error was quantified by comparing the distance between adjacent markers on a single cluster in the first frame of data against the distance between the same two markers in the final frame of data. This was calculated for each of the six clusters.

Application to Comminuted and Repaired Distal Tibia–Fibula Complexes

Two comminuted specimens with both a vertical and transverse wedge fracture were tested to evaluate the technique's ability to capture three types of motions: normal strains, shear strains, and wedge angulations. To quantify the strain at each fracture line, marker clusters were placed on the fragments on either side of the fracture to allow for a local coordinate system to be established on each fragment. Virtual points were then digitized on either side of the fracture gap at both the proximal and distal ends (Fig. 4). As the mating talus was not accessible, an artificial talus was made using dental cement (Denstone Golden, Heraeus Kulzer, South Bend, IN, USA) by creating a mold of the articular surface in order to distribute the applied load evenly. The specimens were loaded from the artificial talus (axially) cyclically at a rate of 0.1 mm/s between 100 and 400N for 10 cycles using a material testing machine (Instron 5967, Norwood, MA, USA), and the optical tracking system recorded the positions of the marker clusters on each of the

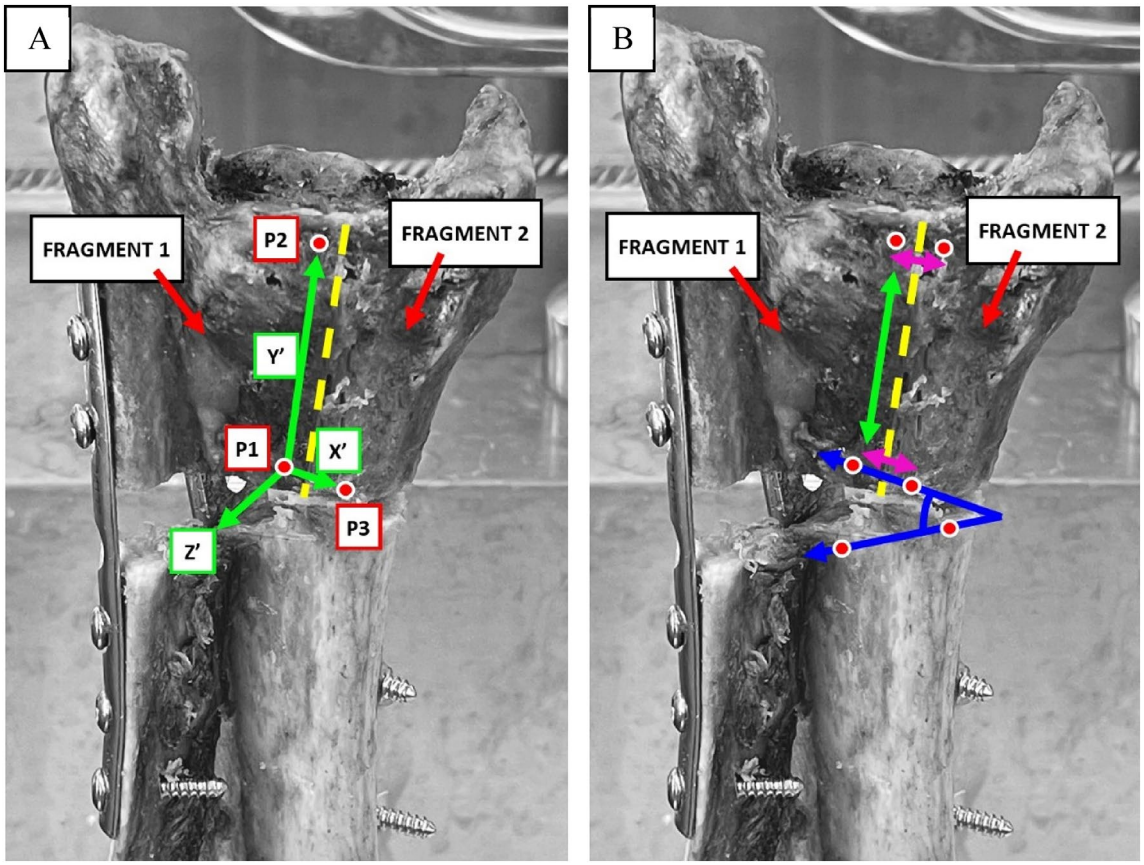

Fig. 4 **a** The anatomic coordinate system X' Y' Z' was created by finding $\boldsymbol{P}_{1\to2}$ to define the Y' axis. The temporary X' axis was defined as $\boldsymbol{P}_{1\to3}$. The cross-product of $\boldsymbol{P}_{1\to3}$ and $\boldsymbol{P}_{1\to2}$ was calculated to define the Z' axis. Finally, the cross-product of Y' and Z' was used to define the true X' axis. **b** The yellow line represents the fracture gap, and the red points represent the positions of the virtual markers. The blue arrows represent the vectors used to calculate the wedge angle. The purple arrows represent normal strains, and the green arrow represents the vertical shear strain.

bone fragments in the global coordinate system at a rate of 120 FPS. Assuming that each bone fragment was rigid and non-deformable meant that the position of each virtual point with respect to its fragment's local coordinate system was constant and each point could be transformed into the global coordinate system for every subsequent frame of data.

An anatomic coordinate system was created at the fracture gap in order to convert the global interfragmentary motions into anatomically relevant motions (as compressive strains, shear strains, and angular displacements). This anatomic coordinate system was based on a vector connecting two virtual points along the fracture gap, which was kept as the *y*-axis of the anatomical coordinate system. A second vector was created using virtual points on either side of the fracture gap at the proximal end. A cross-product between these two vectors produced the *z*-axis of the anatomical coordinate system directed away from the specimen. Finally, the cross-product between the *y*-axis and *z*-axis created the x-axis of the anatomic coordinate system, oriented normal to the fracture gap. (Fig. 4).

The normal and shear strains were computed at the proximal and distal ends of a fracture line. The relative motion between two virtual points on adjacent bone fragments was determined by subtracting the distance between the two points in one frame from the distance between the two points in the following frame. Using a transformation matrix, this displacement vector was projected onto the anatomical coordinate system developed previously in such a way that the x-component of the interfragmentary motion corresponded to compressive movements normal to the fracture gap and the *y*-component of the displacement corresponded to interfragmentary shear movements along the fracture gap. Therefore, the normal and vertical shear strain components were then evaluated individually by dividing the magnitude of the relative motion between the fragments by the initial size of the fracture gap. The initial size of the fracture gap was taken to be the width of the saw blade used to create the fractures (0.58 mm).

In addition to normal and shear strain, angular displacements were also calculated. A vector parallel to the top and bottom edges of the wedge fracture was created using the virtual points and the angle between these two vectors was calculated using the dot product. MATLAB (MATLAB_R2020a, MathWorks, Natick, MA) was used to compute all interfragmentary motions and strains.

Results

Error Analysis

When considering all measurements taken in both the horizontal and vertical directions at nine locations in the transverse plane and three different heights, the optical tracking system had an overall error (SD) of 0.05 (0.08) mm compared to the micrometer (Table 1). More specifically, there was an error (SD) of 0.05 (0.09) mm, 0.08 (0.08) mm, and 0.03 (0.04) mm at the lowest, middle, and highest heights, respectively. Horizontal measurements had an error (SD) of 0.03 (0.05) mm, while vertical measurement errors (SD) were 0.08 (0.10) mm.

Substantially larger errors were seen in the corners of the calibrated testing area. When focused on the primary regions in which a repaired specimen would be located during testing (locations 2, 4, 5, 6, and 8), the overall error (SD) was reduced by 0.03 (0.03) mm. Additionally, there was an error (SD) of 0.02 (0.02) mm, 0.05 (0.04) mm, and 0.02 (0.02) mm at the lowest, middle, and highest height. Horizontal measurements reported an error (SD) of 0.02 (0.02) mm, while vertical measurements reported an error (SD) of 0.04 (0.03) mm.

From the noise assessment, the maximum displacement of the markers during both the static and dynamic tests was 0.01 mm.

When assessing the quality of the custom-made marker clusters, the distance between adjacent markers on a single cluster in the first frame of data and in the final frame of data had an error (SD) of 0.011 (0.008) mm.

Table 1: Results of error analysis between motion capture system and micrometer

Location	Height 1	Height 2	Height 3	All heights
1	5.3	31.3	114.4	50.3
2	19.0	30.6	27.9	25.8
3	196.7	15.3	63.7	91.9
4	13.8	63.1	28.8	35.2
5	13.9	76.6	23.0	37.8
6	21.9	38.6	13.4	24.6
7	0.7	233.9	18.5	84.4
8	37.1	51.0	12.4	33.5
9	144.5	163.3	4.7	104.2
Overall	50.3	78.2	34.1	54.2

All values are in μm

Comminuted Distal Tibia–Fibula Example

The resulting outputs for normal strains, shear strains, and angular displacements using the comminuted distal tibia specimens are shown in Fig. 5.

In terms of the magnitude of the motions presented in Fig. 5, the interfragmentary movements in the normal and vertical shear directions for Specimen 1 were approximately 0.36 mm and 0.21 mm, respectively, and for Specimen 2 were 0.13 mm and 0.13 mm, respectively. For Specimen 1 they increased with cycles, but for Specimen 2 they had generally consistent magnitudes for the ten cycles.

To see the change in the wedge angle during loading rather than the absolute value of the angle, the initial wedge angle (17° and 13° for Specimen 1 and 2, respectively) was subtracted from every frame of data to focus on angular changes such that the initial wedge angle was 0°. The change in wedge angle was detected to be $< 2°$ under the loads applied herein.

Discussion

The main goal of this study was to develop an anatomically relevant 3D tracking technique to assess the relative motion among bone fragments in three motions assessed in benchtop cadaveric studies of fracture repair. Currently, examining 3D fracture gap motion is a new technique such that there has been limited work done in this area. This study was able to develop and validate a technique to track bone interfragmentary movements and resolve them into anatomically meaningful strain values that can be used to estimate a plate's ability to promote bone healing. This could be applied to the development of future plates to provide optimal interfragmentary motion that considers relative motion at every fracture site rather than the overall stiffness response, enhancing patient outcomes post-surgery.

This technique is able to assess the stability and healing potential of comminuted fractures by tracking normal and shear strains, in addition to a wedge gap, which is considered to be an alternate, clinically relevant mode of failure. As shown in Fig. 5, one specimen exhibited a consisted strain magnitude throughout the cyclic loading, while another displayed a consistent drift in the strain measurements. This drift is likely attributable to the poor integrity of the repair and appears as damage accumulates throughout each loading cycle. To validate this technique an error analysis was completed to determine the accuracy of the 3D motion capture system. The overall error was at a minimum in the central region of the capture area (0.03 mm), common in motion capture setups, highlighting the importance of placing a test specimen in this location. Errors may be reduced in the future by optimizing camera positioning to focus on a specific region of interest; in the present study, a relatively large

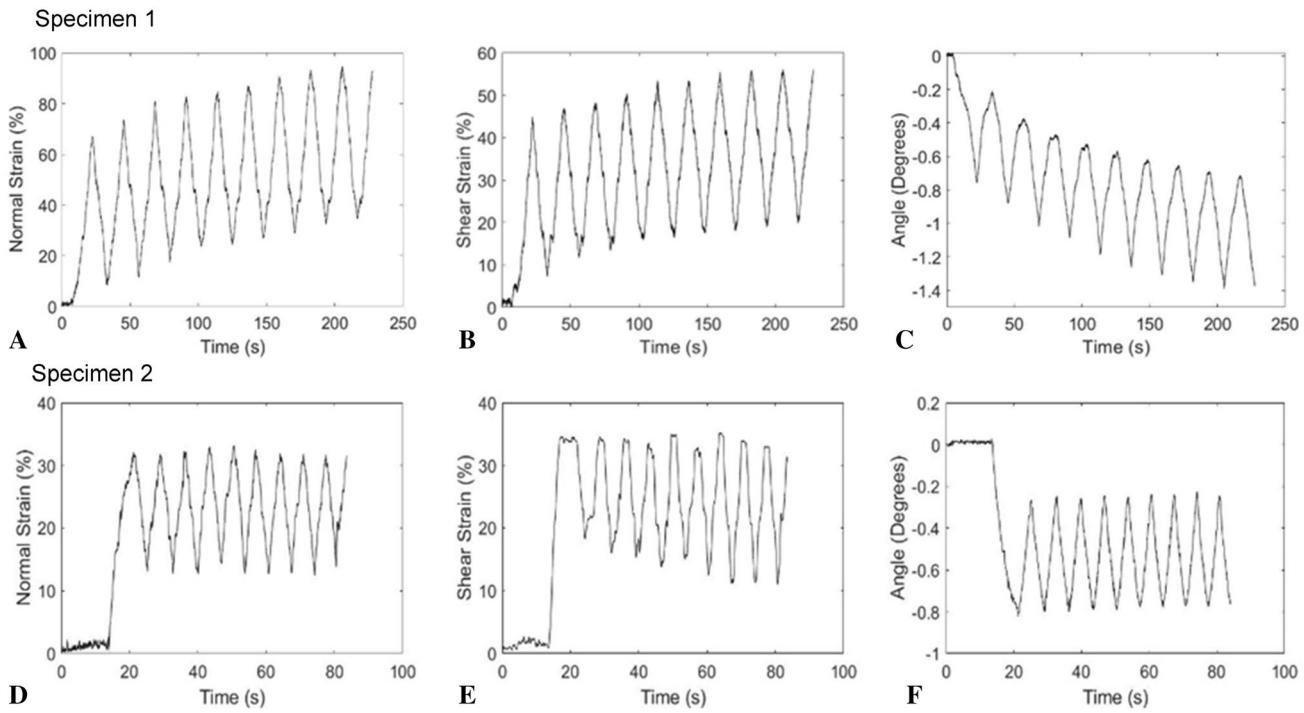

Fig. 5 Plots showing **a**, **d** normal interfragmentary motion in the form of normal strain, **b**, **e** shear interfragmentary motion in the form of shear strain, and **c**, **f** angular interfragmentary motion for two specimens

capture volume was selected to provide the greatest potential range of studies. In addition, the low error from the custom-made marker clusters (0.011 mm) suggests that the clusters behaved reliably and consistently throughout the testing protocol. When using the Instron for stiffness and failure testing, there were vibrations that caused small marker motions (0.01 mm). This vibration analysis test was completed by running the Instron at a constant rate of 0.1 mm/s, which was the rate used for the construct loading tests. The errors measured were approximately 10% of the magnitude being measured, supporting the conclusion that while pushing the capabilities of the system, motion capture can operate at a high accuracy to provide detail on small interfragmentary motions. This has important clinical implications for assessing bone healing during fracture plate design and evaluation.

While common in biomechanics, the use of optical tracking for assessing 3D interfragmentary motion tracking has been limited [6, 15, 24], primarily due to the size of the motions. A study by Muizelaar et al. [20], tested a bilateral plating technique to repair distal femur periprosthetic fractures using 3D motion tracking [20]. They measured fracture motions on the order of 4–20% of fracture gap width, demonstrating that 3D motion tracking could be used for this application. However, that study was on a single, simple transverse fracture under isolated loading directions. Another previous study validated a high-end optical measurement system against a conventional tactile measurement system in the detection of 3D micromotions (less than or equal to 5 μm) [4]. With errors a degree of magnitude lower than those in the present study, it was considered to have high enough resolution for micromotion evaluations; however, was only tested using a simple setup consisting of a tube with a transverse cut in it, and used patches with arrays of markers, which may be difficult to secure to cadaveric bone due to the irregular and moist surface. The Pontos 5 M camera system used in that work had a resolution of 6 Megapixels, which is more than four times that of the present system (at 1.3 Megapixels). It is possible that with higher quality cameras, our system could have lower errors as well; however, the Optitrack represents an affordable system, making this accessible to the average biomechanics group. Finally, no known previous study examined the collection of fracture motion types presented herein, opting to use simplified and more highly controlled (but less realistic) setups.

This technique provides a variety of insights when testing comminuted distal tibial fractured specimens. When evaluating the amount of strain at the fracture site, the initial gap size needs to be considered in addition to the amount of interfragmentary motion. For a smaller initial gap size, a smaller amount of interfragmentary motion can be tolerated in order to reach an acceptable level of strain to promote healing, and as such may test the performance limits of the present system. As previously mentioned, the interfragmentary movements for Specimen 1 in the normal and vertical shear directions were approximately 0.36 mm and 0.21 mm, respectively, and for Specimen 2 were 0.13 mm and 0.13 mm, respectively. For Specimen 1, this is within the suggested range for axial interfragmentary motion (i.e., 0.2 to 1 mm) that is required for early secondary bone healing [1, 5, 13]. For Specimen 2, the movements were small even smaller than the optimal range for secondary healing, hence, this fractured specimen is considered to be more stable than the first specimen. Similarly, another study used finite element analysis to predict interfragmentary movement and found that axial movement ranged between 0.1 and 1.3 mm, while shear movements were between 0.2 mm and 0.5 mm [19]. Also, to prevent delayed healing, the ratio between the shear interfragmentary motion (SIM) and axial interfragmentary motion (AIM) must be less than 1.6 [23]. From the results, the SIM/AIM ratio was in fact less than 1.6, which signifies that delayed healing can be prevented. This information can be used clinically to understand how a treatment performs post-surgery. It also provides vital information on the success of the treatment that relies on adequate healing.

Also, previous studies determined and were able to calculate interfragmentary movements at the fracture site using three-dimensional tracking on sheep's tibia [15, 16]. They found that for first group, the interfragmentary movements were out of the appropriate range for healing, this caused initial instability which was important as large movements in the initial healing stage caused a delay in callus formation [15]. In addition, another study found that 3D fracture site motion would be a better predictor of callus formation compared to stiffness [8, 25], and as such this new technique to track the amount of interfragmentary motion at the fracture site has great clinical relevance. However, this research had some limitations. To track the positions of virtual points on each fragment on a bone, it was assumed that each fragment was a rigid body and did not deform. Although bone is deformable and anisotropic, this was a necessary assumption to simplify the analysis. This is further supported by the fact that bone deformations were substantially smaller than the movements at the fracture gap [17]. This technique has significant clinical importance; however, it is mainly for research and development purposes to develop optimized fracture plates to enhance healing, and as with all benchtop studies, represents only the immediate post-surgical healing condition. Furthermore, this robust technique can also be applied to a broad range of fracture healing scenarios (beyond the pilon fracture examples presented herein) to improve our understanding of how best to promote healing.

Overall, this study was able to develop a technique to track three-dimensional interfragmentary motions at different types of fracture sites and resolve them into normal and shear components for anatomically relevant outcomes,

while a repaired bone construct was loaded to simulate the immediate post-repair condition for healing. The outcome of the study demonstrated that this is an affordable system to implement in biomechanical laboratories to support the development and evaluation of future fracture treatments.

Acknowledgments This research had no technical help, no contributions that do not justify authorship, and no financial relationships that pose a conflict of interest. All the equipment and specimens were purchased and funded using CQ's NSERC Discovery grant. DePuy Synthes donated the fracture plates through a Johnson & Johnson Investigator Initiated Study.

Declarations

Conflict of interest Ali Ammar, Andrew Koshyk, Marisa Kohut, Bashar Alolabi, and Cheryl Quenneville declare they have no conflict of interest.

References

1. Bottlang, M., J. Doornink, D. C. Fitzpatrick, and S. M. Madey. Far cortical locking can reduce stiffness of locked plating constructs while retaining construct strength. *J. Bone Joint Surg. (Am)*. 91:1985–1994, 2009.
2. Claes, L. E., C. A. Heigele, C. Neidlinger-Wilke, D. Kaspar, W. Seidl, K. J. Margevicius, and P. Augat. Effects of mechanical factors on the fracture healing process. *Clin. Orthop. Related Res.* 355S:S132–S147, 1998.
3. Doblaré, M., J. M. García, and M. J. Gómez. Modelling bone tissue fracture and healing: a review. *Eng. Fracture Mech.* 71(13–14):1809–1840, 2004.
4. Doebele, S., S. Siebenlist, H. Vester, et al. New method for detection of complex 3D fracture motion—verification of an optical motion analysis system for biomechanical studies. *BMC Musculoskelet. Disord.* 13:33, 2012.
5. Doornink, J., D. C. Fitzpatrick, S. M. Madey, and M. Bottlang. Far cortical locking enables flexible fixation with periarticular locking plates. *J. Orthop. Trauma*. 25:S29–S34, 2011.
6. Duda, G. N., M. Sollmann, S. Sporrer, J. E. Hoffmann, J. Kassi, C. Khodadadyan, and M. Raschke. Interfragmentary motion in tibial osteotomies stabilized with Ring fixators. *Clin. Orthop. Relat. Res.* 396:163–172, 2002. https://doi.org/10.1097/00003086-200203000-00025.
7. Egol, K. A., E. N. Kubiak, E. Fulkerson, F. J. Kummer, and K. J. Koval. Biomechanics of locked plates and screws. *J. Orthop. Trauma*. 18(8):488–493, 2004.
8. Elkins, J., J. L. Marsh, T. Lujan, R. Peindl, J. Kellam, D. D. Anderson, and W. Lack. Motion predicts clinical callus formation: construct-specific finite element analysis of supracondylar femoral fractures. *J. Bone Joint Surg. Am.* 98(4):276–284, 2016.
9. Elliott, D. S., K. J. H. Newman, D. P. Forward, D. M. Hahn, B. Ollivere, K. Kojima, R. Handley, N. D. Rossiter, J. J. Wixted, W. Smith, and R. M. Moran. A unified theory of bone healing and nonunion. *Bone Joint J.* 98(7):884–891, 2016.
10. Ganse, B., P.-F. Yang, G.-P. Brüggemann, L. P. Müller, J. Rittweger, and T. Koy. In vivo measurements of human bone deformation using optical segment tracking: surgical approach and validation in a three-point bending test. *J. Musculoskelet. Neuronal Interact.* 14(1):95–103, 2014.
11. Goodship, A. E., J. L. Cunningham, and J. Kenwright. Strain rate and timing of stimulation in mechanical modulation of fracture healing. *Clin. Orthop. Relat Res*. 355:S105–S115, 1998.
12. Harwood, P. J., J. B. Newman, and A. L. R. Michael. An update on fracture healing and non-union. *Orthop. Trauma*. 24(1):9–23, 2010.
13. Jagodzinski, M., and C. Krettek. Effect of mechanical stability on fracture healing—an update. *Injury*. 38(S1):S3–S10, 2007.
14. Kaspar, K., H. Schell, P. Seebeck, M. Thompson, M. Schütz, N. Haas, and G. Duda. Angle stable locking reduces interfragmentary movements and promotes healing after unreamed nailing. *J. Bone Joint Surg.* 87(9):2028–2037, 2005. https://doi.org/10.2106/jbjs.d.02268.
15. Klein, P., M. Opitz, H. Schell, W. R. Taylor, M. O. Heller, J. Kassi, F. Kandziora, and G. N. Duda. Comparison of unreamed nailing and external fixation of tibial diastases—mechanical conditions during healing and biological outcome. *J. Orthop. Res.* 22(5):1072–1078, 2004. https://doi.org/10.1016/j.orthres.2004.02.006.
16. Klein, P., H. Schell, F. Streitparth, M. Heller, J. Kassi, F. Kandziora, N. P. Haas, and G. N. Duda. The initial phase of fracture healing is specifically sensitive to mechanical conditions. *J. Orthop. Res.* 21(4):662–669, 2003. https://doi.org/10.1016/s0736-0266(02)00259-0.
17. Märdian, S., W. Schmölz, K.-D. Schaser, G. N. Duda, and M. Heyland. Locking plate constructs benefit from interfragmentary lag screw fixation with decreased shear movements and more predictable fracture gap motion in simple fracture patterns. *Clin. Biomech.* 70:89–96, 2019.
18. Marsell, R., and T. A. Einhorn. The biology of fracture healing. *Injury*. 42(6):551–555, 2011.
19. Mühling, M., M. Winkler, and P. Augat. Prediction of interfragmentary movement in fracture fixation constructs using a combination of finite element modeling and rigid body assumptions. *Comput. Methods Biomech. Biomed. Eng.* 24(15):1752–1760, 2021. https://doi.org/10.1080/10255842.2021.1919883.
20. Muizelaar, A., M. J. Winemaker, C. E. Quenneville, and G. R. Wohl. Preliminary testing of a novel bilateral plating technique for treating periprosthetic fractures of the distal femur. *Clin. Biomech.* 30(9):921–926, 2015.
21. Pirolo, J. M., A. W. Behn, G. D. Abrams, and J. A. Bishop. Anterolateral versus medial plating of distal extra-articular tibia fractures: a biomechanical model. *Orthopedics*. 38(9):e760–e765, 2015.
22. Remedios, A. Bone and bone healing. *Fract. Manage. Bone Heal.* 29(5):1029–1044, 1999.
23. Schell, H., D. R. Epari, J. P. Kassi, H. Bragulla, H. J. Bail, and G. N. Duda. The course of bone healing is influenced by the initial shear fixation stability. *J. Orthop. Res.* 23(5):1022–1028, 2005.
24. Schell, H., M. S. Thompson, H. J. Bail, J. Hoffmann, A. Schill, G. N. Duda, and J. Lienau. Mechanical induction of critically delayed Bone Healing in sheep: Radiological and biomechanical results. *J. Biomech.* 41(14):3066–3072, 2008. https://doi.org/10.1016/j.jbiomech.2008.06.038.
25. Seebeck, P., M. Thompson, A. Parwani, W. Taylor, H. Schell, and G. Duda. Gait evaluation: a tool to monitor bone healing? *Clin. Biomech.* 20(9):883–891, 2005. https://doi.org/10.1016/j.clinbiomech.2005.05.010.
26. Warden, S. J., and C. H. Turner. Mechanotransduction in cortical bone is most efficient at loading frequencies of 5–10 Hz. *Bone*. 34:261–270, 2004.
27. Wraighte, P., and B. Scammell. Principles of fracture healing. *General Princ. Orthop. Surg.* 24(6):198–207, 2006.
28. Yenna, Z. C., A. K. Bhadra, N. I. Ojike, A. ShahulHameed, R. L. Burden, M. J. Voor, and C. S. Roberts. Anterolateral and medial

locking plate stiffness in distal tibial fracture model. *Foot & Ankle Int.* 32(6):630–637, 2011.